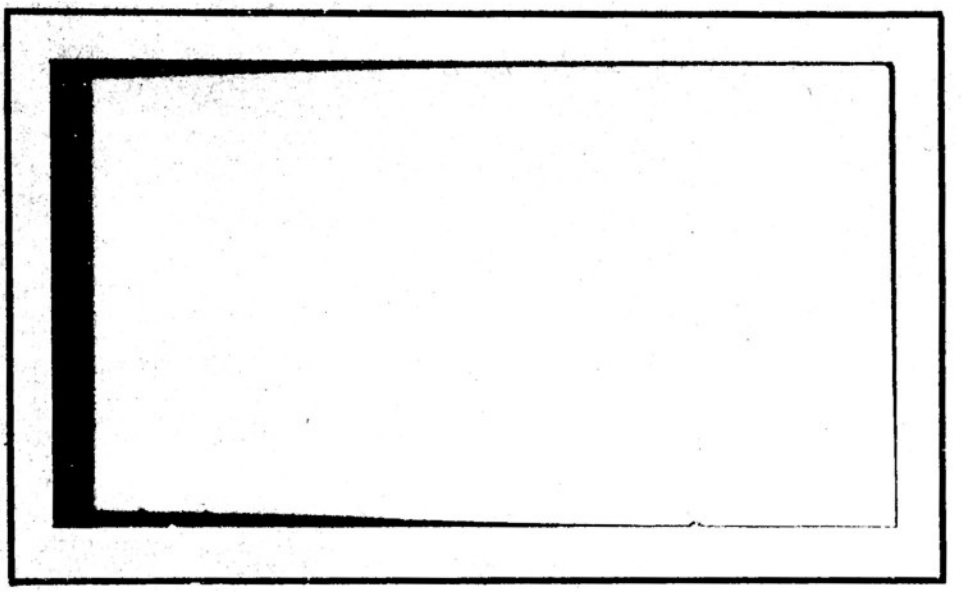

OFFICE OF NAVAL RESEARCH

and

ATOMIC ENERGY COMMISSION

Contract N6 ori-83, T. O. II

NR 024-022

Nuclear Physics Laboratory

UNIVERSITY OF NOTRE DAME

NOTRE DAME, INDIANA

NUCLEAR PHYSICS

TECHNICAL REPORT NO. 3

Photodisintegration Thresholds of Deuterium and Beryllium

J. C. Noyes, J. E. VanHoomissen

W. C. Miller, and B. Waldman

OFFICE OF NAVAL RESEARCH

and

ATOMIC ENERGY COMMISSION

Contract N6 ori-83, T. O. II

NR 024-022

UNIVERSITY OF NOTRE DAME

DEPARTMENT OF PHYSICS

NOTRE DAME, INDIANA

November 1953

Abstract

The photodisintegration thresholds of deuterium and beryllium have been determined by using the bremsstrahlung produced by monoergic electrons. The energy of the electrons was measured with a cylindrical electrostatic analyzer to an accuracy of 0.1%. The binding energy of deuterium was found to be 2.227 ± 0.003 Mev and that of beryllium was found to be 1.662 ± 0.003 Mev.

I INTRODUCTION

The photodisintegration thresholds of deuterium and beryllium have been measured using a number of methods. Stephens[1], in 1947, presented an exhaustive discussion of the work done on deuterium up to that time. Since 1948 two important experiments have been performed.

Bell and Elliot[2] measured the energy of the gamma ray accompanying the capture of a neutron by a proton. Their spectrometer was calibrated with the 2.615 ± 0.001 Mev gamma ray[3] of ThC". Their value for the binding energy of the deuteron is 2.230 ± 0.007 Mev.

Mobley and Laubenstein[4] determined the photodisintegration thresholds of beryllium and deuterium with a novel method. Using the Argonne National Laboratory electrostatic generator, they had a proton beam accelerated down the normal accelerator tube while an electron beam was accelerated up the differential pumping tube to the high voltage electrode. The electrons were stopped in a gold target, producing x-rays which were used for the photodisintegration. Energy calibration was accomplished by comparison with the Li(p,n) threshold[5], known to ± 0.1%. The values obtained for the binding energies of beryllium and deuterium are respectively, 1.666 ± 0.002 Mev and 2.226 ± 0.003 Mev.

The present experiment was undertaken because it is the most direct method for determining the binding energies. It is an absolute method requiring no nuclear reaction data for calibration.

II EXPERIMENTAL ARRANGEMENT

The photodisintegration thresholds of beryllium and deuterium were determined as follows: Electrons from the electrostatic generator entered a 90-degree electrostatic analyzer, which served as an energy selector. The electrons which emerged from the analyzer struck a thick gold target, producing a continuous x-ray spectrum with an upper energy limit equal to the electrons' energy. The x-rays above threshold disintegrated the beryllium or deuterium, producing neutrons. The neutron yields at various electron energies up to 30 kev above threshold were extrapolated to zero yield. On converting the energy corresponding to zero yield into the center-of-mass system, the binding energies of beryllium and deuterium were obtained.

The maximum undertainty in threshold energy as determined by this experiment is 0.1%. To realize this accuracy, the uncertainties in individual measurements contributing to the threshold measurement had to be kept well below this value. The final energy measurement depended only upon an accurate knowledge of the geometry of the analyzer system, and the determination of the deflecting voltage.

A. Electrostatic Analyzer

Since the heart of this experiment was the electrostatic analyzer, it will be described in detail.

The theory of the electrostatic analyzer has been adequately reviewed by Bainbridge[6]. Honnold and Miller* [7] have developed the

*Cf. Accompanying Technical Report

relativistic ion optics of an electrostatic analyzer with application to this particular analyzer. They have shown that electrons of kinetic energy T_o and velocity $\beta_o c$ emerging from an object slit (Cf. Fig. 1) placed a distance ℓ' from the entrance to the field O' will be imaged at a distance ℓ'' from the exit from the field O'' given by the lens equation

$$(\ell' - g)(\ell'' - g) = f^2 \qquad \text{(HM-24)} \quad (1)$$

where

$f = \frac{a}{\kappa \sin \kappa \Phi}$ = focal length

$g = f \cos \kappa \Phi$ = coordinates of focal points

$\kappa = \sqrt{1 - \beta_o^2}$

a = mean line trajectory

provided the potential difference X between the plates P_1 and P_2 is

$$X = \frac{T_o}{e}\left(\frac{T_o + 2R}{T_o + R}\right)\frac{d}{a} \qquad \text{(HM-2b)} \quad (2)$$

where

R = rest energy of electron

d = separation of plates.

Furthermore, the energy resolution is determined by the width of the slits in the object and image planes, W' and W'' respectively. For the case where these widths are in the ratio of the lateral magnification of the lens the resolution is given by

$$\left(\frac{dT}{T_o}\right) = \left(\frac{T_o + 2R}{T_o + R}\right)\frac{W''}{a(1-M)} \qquad \text{(HM-31)} \quad (3)$$

where dT is the energy increment needed to displace the image beyond

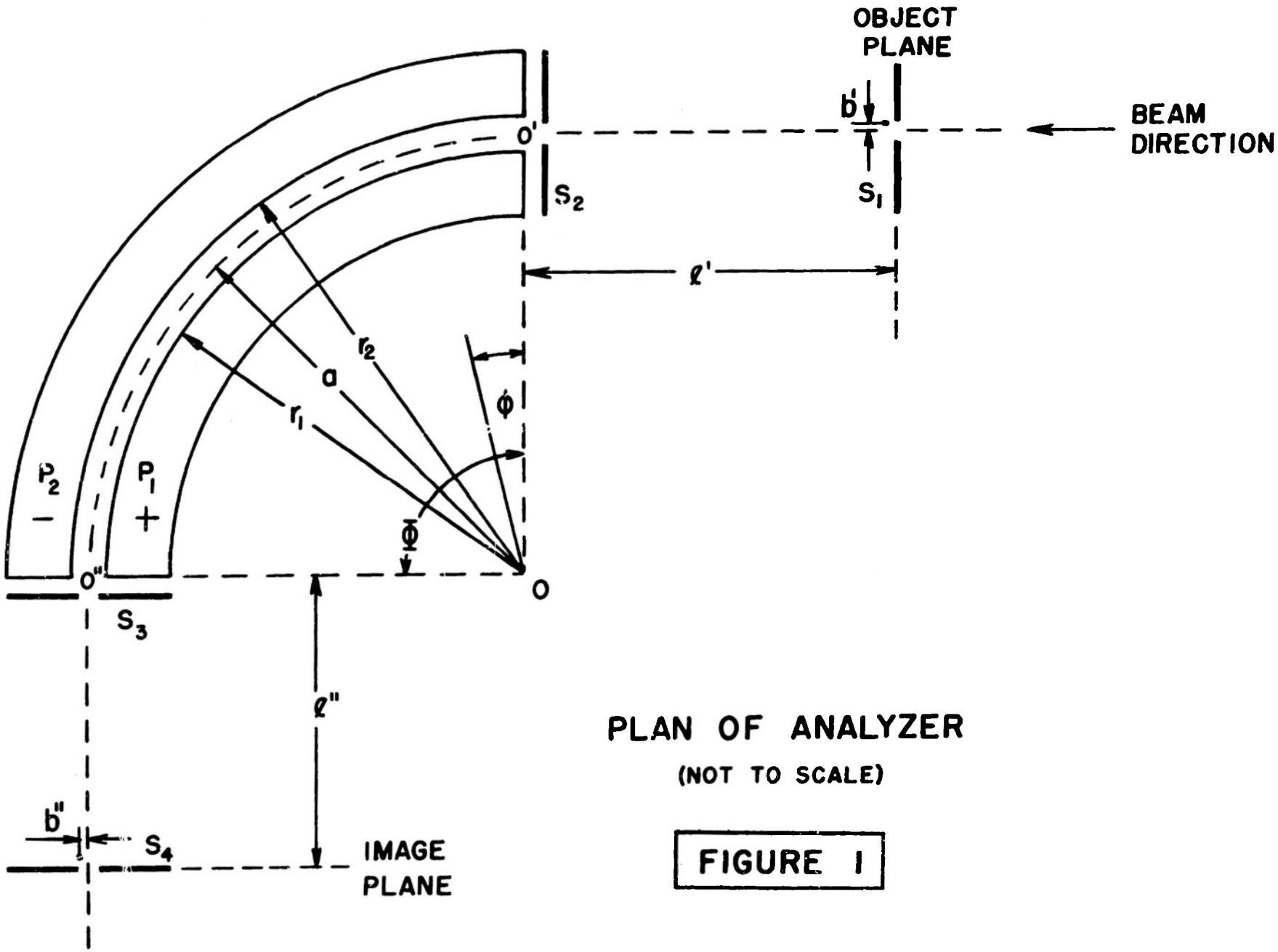

PLAN OF ANALYZER

(NOT TO SCALE)

FIGURE 1

the slit W'' and M is the lateral magnification .

The dimensions of the analyzer were based on the available laboratory space and the required deflection voltage. The voltage depended on the separation of the plates and their mean radius, from eq. 2. Furthermore, the separation had to be large enough so that the beam would not strike the plates. A separation of 5/16" and mean radius o. 24" were used. The angle Φ was made 90° on the basis of ease of construction and direction of exit beam. This angle was in a horizontal plane. Since ℓ' and ℓ'' are functions of energy, it was decided in the interest of mechanical simplicity to fix one and vary the other. The object distance ℓ' was set at 30". The values of ℓ'' at 1.67 and 2.22 Mev were 16.65" and 17.54" respectively.

The two analyzer plates P_1 and P_2 were cut from one piece of steel. In cross section they were 1 3/16" thick and 2 1/4" wide, and subtended an angle of 90° at point O in Figure 1. For a thickness of 1 3/16", the electric field lines between the two plates were practically parallel in a 1/4" thick region in the center of the plates. This figure of 1/4" was estimated to be the maximum beam thickness. The plates were supported on 6 Mykroy cylinders, 1 1/2" diameter by 1 1/4" long, to the ends of which were cemented 1/4" cylindrical steel end pieces. The lower end pieces were fastened to a 30" by 36" steel surface plate, flat to 0.001". The upper end pieces were tapped, and to these were bolted the analyzer plates. Clearance was provided in the bolt holes through the analyzer plates so that the position of the plates could be

adjusted slightly.

There were four pairs of beam-defining slits used with the analyzer. The object slits, S_1, were in the object plane, 30" from the entrance end of the analyzer. Two pairs of slits, S_2 and S_3, were located at the entrance and exit ends of the analyzer, and were spaced 0.100" from the ends of the analyzer plates. Slits S_2 and S_3 served to define the electric field at the ends of the analyzer.

It has been shown[8] that by proper placement of slits S_2 and S_3 the effect of the fringe field at the ends of the analyzer could be completely nullified; that is, the electric field outside the analyzer plates could be considered equal to zero.

The fourth pair of slits, S_4, was in the image plane. Since the object distance was fixed at 30", the image distance varied with beam energy. Provision was made to vary the distance of S_4 from the analyzer by means of a carriage driven by a screw.

A vacuum housing of 1/8" thick brass enclosed the analyzer plates and S_2 and S_3. This housing, having the same angular contour as the analyzer plates, was 4" high by 7" wide, and extended 1½" beyond either end of the analyzer plates. A 1/8" rubber gasket around the bottom of the housing provided the necessary vacuum seal.

The object slits were located in a cylindrical slit chamber, which was connected to the analyzer housing by means of a 1" brass pipe and a short sylphon section.

At the exit end of the analyzer housing was another sylphon section, to which was attached a section of 2" brass pipe. Concentric with this pipe was another brass pipe 1½" in diameter, to which was attached a rectangular slit chamber containing the

image slits. The vacuum seal between the two pipes was provided by an O-ring inside the larger pipe. A screw-driven carriage permitted motion of the exit slit chamber in two directions. First, motion in the direction of the beam was permitted by the telescoping action of the concentric pipes. A total movement of four inches was obtainable, this being the change in image distance with a change of beam energy from 1 Mev to 3 Mev. Secondly, a movement of the image slit chamber transverse to the beam direction was obtainable by another screw mechanism. This movement was permitted by the sylphon at the end of the analyzer housing, and was necessary for the alignment of S_4.

Each slit consisted of two pieces of tantalum, 0.040" thick, mounted on and insulated from an adjustable screw-driven mechanism which permitted the separation to be varied without changing the slit center line. The control shafts extended downward, through the slit chambers in the case of slits S_1 and S_4, and through the surface plate for slits S_2 and S_3. O-rings provided the vacuum seals. The slits were connected to ground through microammeters located in the control room.

Vacuum was maintained in the system by a National Research Corporation H2P diffusion pump, type 113, backed by a Cenco Hypervac 20 forepump. A pressure of 1×10^{-5} mm Hg was maintained in the system with no beam through the analyzer. A liquid-air trap was located between the pump and analyzer.

B. Alignment

The inner analyzer plate P_1 was bolted into place on its

three Mykroy insulators and two sets of measurements were made on the surface of radius r_1. First, relative variations of the radius of curvature at three different depths from the top surface of the analyzer were obtained by means of a travelling dial gauge moving perpendicularly to the surface plate. The dial gauge was zeroed at a position 1/8" from the top of the analyzer, then readings were taken at a position 5/8" from the top (center of analyzer) and at a position 1 1/16" from the top surface. The measuring apparatus was then moved to another angular position, the gauge re-zeroed at the 1/8" depth, and deviations again noted at the other two depths. These sets of three relative measurements were made at a total of eleven angular positions, approximately 9° apart. Data are recorded in Table 1.

The second set of measurements on this surface was a determination of the variation of radius of curvature as a function of angular displacement from the entrance end, the variations in radius being measured relative to the entrance end. The travelling dial gauge was fastened to the radius arm pivoted at O, Figure 1, and was zeroed at a point 1/8" below the top of the analyzer plate at the entrance end (0°). Variations from zero were then observed at the ten other angular positions previously mentioned, all at the same depth of 1/8". These data are recorded in Table 2.

The data of Table 2 served to redefine the zeroes of Table 1. Hence one could compute the relative variations of radius from a point 1/8" below the top of the analyzer plate at the entrance end.

The outer analyzer plate P_2 was then moved into position and separated from the inner plate by three machined steel spacers, of

Table 1

Variations in radius of curvature of inner plate at 3 different depths from top of plate. (- sign indicates a decrease of radius)

Angle from entrance, θ	Radius Variations at different depths from top (inches)		
	1/8"	5/8"	1 1/16"
	x 10^{-4}	x 10^{-4}	x 10^{-4}
0°	0	-1.3	-3.3
9.5°	0	-1.6	-2.9
19.3°	0	-2.5	-3.7
27.9°	0	-1.3	-2.9
37.4°	0	-2.0	-3.5
46.6°	0	-1.3	-2.6
56.3°	0	-1.4	-2.8
65.6°	0	-1.4	-2.8
74.6°	0	-1.3	-2.6
84.9°	0	-0.7	-2.0
89.1°	0	-1.7	-3.2

Table 2

Variations in radius of curvature of inner plate at constant depth below top of plate (1/8"). (+ sign indicates an increase of radius)

Angle from entrance, θ	Radius Variations (inches)		
	Trial 1	Trial 2	Average
	x 10^{-4}	x 10^{-4}	x 10^{-4}
0°	0	0	0
9.5°	+1.6	+1.5	+1.6
19.3°	+4.9	+5.0	+5.0
27.9°	+7.0	+7.0	+7.0
37.4°	+7.5	+7.5	+7.5
46.6°	+7.6	+7.5	+7.6
56.3°	+6.0	+6.0	+6.0
65.6°	+4.7	+4.8	+4.8
74.6°	+3.5	+3.3	+3.4
84.9°	+1.1	+1.3	+1.2
89.1°	+0.5	+0.5	+0.5

Table 3

Variations in radius of curvature of outer plate at constant depth (1/8") below top of plate. (+ sign indicates an increase of radius)

Angle from entrance, θ	Radius Variation (inches)		
	Trial 1	Trial 2	Average
	x 10^{-4}	x 10^{-4}	x 10^{-4}
0°	0	0	0
9.5°	+3.2	+3.1	+3.2
19.3°	+6.1	+6.0	+6.0
27.9°	+6.8	+6.7	+6.8
37.4°	+6.8	+6.8	+6.8
46.6°	+6.9	+6.8	+6.8
56.3°	+6.8	+6.8	+6.8
65.6°	+5.9	+5.9	+5.9
74.6°	+3.8	+3.7	+3.8
84.9°	+1.5	+1.2	+1.4
89.1°	+0.0	-0.5	-0.2

Table 4

Combination of variations of Tables 1, 2, & 3 to obtain separation of plates.

Angle	Corrections to be added to separation of 30420 x 10^{-5} in.			
	1/8" depth			
	From Table 1	From Table 2	From Table 3	Net Correction
0°	0	0	0	0
9.5°	0	-16	32	16
19.3°	0	-50	60	10
27.9°	0	-70	68	- 2
37.4°	0	-75	68	- 7
46.6°	0	-76	68	- 8
56.3°	0	-60	68	8
65.6°	0	-48	59	11
74.6°	0	-34	38	4
84.9°	0	-12	14	2
89.1°	0	- 5	- 2	- 7
	5/8" depth			
0°	13	0	0	13
9.5°	16	-16	32	32
19.3°	25	-50	60	35
27.9°	13	-70	68	11
37.4°	20	-75	68	13
46.6°	13	-76	68	5
56.3°	14	-60	68	22
65.6°	14	-48	59	25
74.6°	13	-34	38	17
84.9°	7	-12	14	9
89.1°	17	- 5	- 2	10
	1 1/16" depth			
0°	33	0	0	33
9.5°	29	-16	32	45
19.3°	37	-50	60	47
27.9°	29	-70	68	27
37.4°	35	-75	68	28
46.6°	26	-76	68	18
56.3°	28	-60	68	36
65.6°	28	-48	59	39
74.6°	26	-34	38	30
84.9°	20	-12	14	22
89.1°	32	- 5	- 2	25

0.3042" thickness. The plate was adjusted for a snug fit of the spacers, then was bolted down and the spacers removed. The same measurements that were previously made on the inner plate were then made on the surface of radius r_2. This outer plate had been machined much more accurately than the inner plate, as no variations in radius from upper to lower position could be detected. The variations in radius as a function of angle at a depth of 1/8" from the top surface are recorded in Table 3.

Assuming then that the separation of the two plates at the top at 0° was 0.3042", one could compute the separation between the two plates at the eleven angular positions and at three different depths from the top of the analyzer plates. These computations are recorded in Table 4 and in the graph of Figure 2. From this graph the separation of the plates in the usable portion of the analyzer (5/8" depth) was taken as 0.3044 $\pm$ 0.05%.

Absolute measurement of the radius of curvature of the inner plate was made with a cathetometer. The cathetometer was clamped to the surface plate, the graduated rod parallel to the line 00" in Figure 1. The telescope was first focused on the inner edge of one of the machined spacers between the two analyzer plates at 0" just above the top of the plates. Recording this scale reading, the telescope was next focused on a marker on the radius arm at the same height as the top of the analyzer plates, and on the line 00". The radius arm was then rotated 180° and the marker again found in the telescope cross-hairs. The average of this reading and the preceding one was taken as the reading that would have been obtained if it were possible to find the point 0 when viewing in the plane of the analyzer. These measurements were repeated and

FIGURE 2

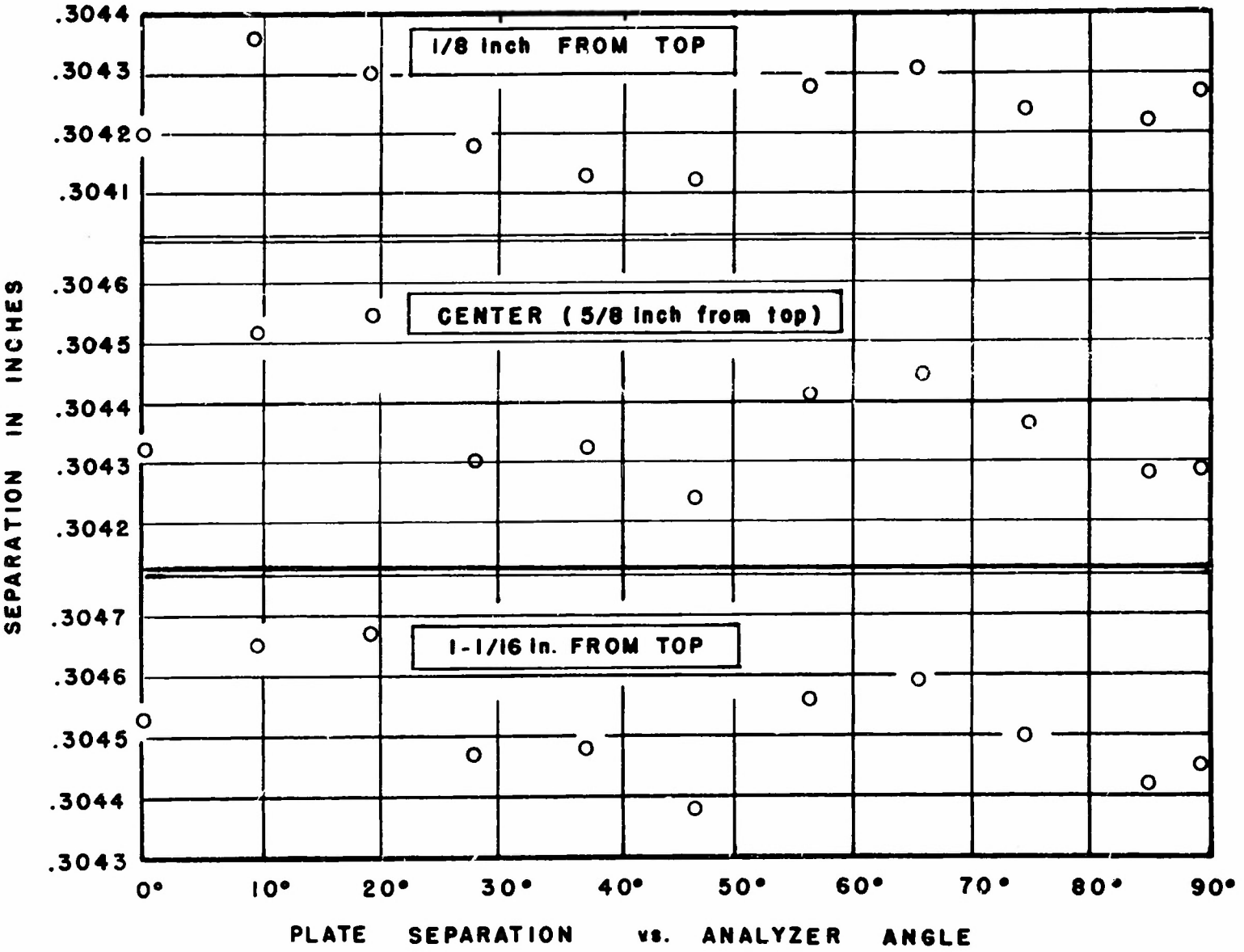
.3044
.3043
.3042
.3041
1/8 inch FROM TOP
.3046
.3045
.3044
.3043
.3042
CENTER (5/8 inch from top)
.3047
.3046
.3045
.3044
.3043
1-1/16 In. FROM TOP
SEPARATION IN INCHES
0°
10°
20°
30°
40°
50°
60°
70°
80°
90°
PLATE SEPARATION vs. ANALYZER ANGLE

an average taken (Table 5). The inner radius r_1 is 23.851" $\pm$ 0.005%. The outer radius r_2 is 23.851" + 0.304" = 24.155 $\pm$ 0.005%, and the arithmetic mean radius is 24.003" with a liberal error of 0.01%. The geometric mean radius a is $\sqrt{(23.851)(24.155)}$ = 24.002" $\pm$ 0.01%. Note that at this percentage error (a) the arithmetic and geometric mean radii are equal, and (b) the variations of radius as given in Table 1 through 4 do not appear.

Table 5

Determination of radius r_1 by cathetometer measurements.				
Reading at analyzer exit	Reading of marker on radius arm	Reading on radius arm after rotating 180°	Average Columns 2 & 3	Difference Columns 1 & 4
846.9 mm	281.9	200.3	241.1	605.8
846.9	281.7	200.3	241.0	605.9
846.8	281.3	200.3	241.05	605.75
846.9	281.9	200.3	241.1	605.8
			Average	605.8 $\pm$ 0.06 = 605.8 $\pm$ 0.01% millimeters
Radius r_1 at exit end is 605.8 $\pm$ 0.01% mm = 23.851 $\pm$ 0.01% inches.				

The next alignment step was the location of the entrance slit S_1 on a line tangent to the arc 0'0" and perpendicular to the line 00'. This was done by triangulation. Since the distances 00' (24.002") and 0'S_1 (30.000") were known, the distance 0S_1 was calculated as $\sqrt{(24.002)^2 + (30.000)^2}$ = 38.420".

The cathetometer was clamped to a framework erected above the analyzer. A system of levels insured that the calibrated rod was horizontal and the telescope vertical for all measurements. The cathetometer was first aligned in the direction 0'S_1, a reading

taken at 0', and the telescope then moved 30.00" toward S_1. The slit S_1 was then closed and the whole slit assembly moved until the junction of the tantalum pieces on the analyzer side appeared under the cross-hairs. The cathetometer was next aligned in the direction OS_1, a reading taken at the point 0 (scribed in the radius arm axis), and the telescope then moved a distance 38.420" toward S_1. The slit assembly was then moved transverse to the line $O'S_1$ until the junction of the tantalum pieces was again under the cross-hairs. The cathetometer was then moved above the line $O'S_1$ to insure that the distance 30.000" had not been changed by the preceding movement.

The location of slits S_2 and S_3 constituted the last of the alignment. Herzog[8] has shown that for an analyzer spacing of 0.304", the fringe field at the ends of the analyzer can be considered equal to zero if the field confining slits are opened to a separation of 0.060" and spaced from the analyzer ends by 0.075". The spacing was adjusted with feeler gauges. However, during the running of the experiment it was found necessary to increase the spacing, due to voltage breakdown from the analyzer plates, and to open slit S_2 wider to permit more beam current to enter the analyzer. The final experimental data were taken with both slits at a distance 0.100" from the analyzer ends, with S_2 opened to 0.075" and S_3 opened to 0.060". The effect of these changes was to increase the effective analyzer angle slightly, due to greater fringing at the ends. The change in analyzer angle causes a slight shift in the image distance l'' and in the magnification M, and hence in the resolution. However, calculation showed that the increment of analyzer angle was 0.012 radians, resulting in a negligible change in the above-mentioned quantities.

Slit S_4 was set at the proper value of ℓ'' (16.65" for beryllium and 17.54" for deuterium) by a screw driven carriage calibrated with a cathetometer. The position of S_4 in the image plane (transverse to the beam) was adjusted so that the beam current passing through it was a maximum. This method of location of S_4 compensates for the increased angle of the analyzer due to the fringe fields.

It can be shown by use of Honnold and Miller's[7] equation (18) that for the particular conditions of this experiment slit S_3 limits the electron beam energy to ± 3 kev. More recently, further experiments to check this method of positioning S_4 were undertaken by Bhattacherjee, Waldman and Miller*[9]. Their data show that the position of slit S_4 for maximum current through it corresponds to the location of S_4 on the tangent line to the circular orbit in the analyzer drawn at the effective end of the electrostatic field.

C. Measurement of Voltage

A tapped resistance voltage divider was placed from each analyzer plate to ground. The potential difference between the plates was computed from the measured potential difference between the two taps. (See Figures 3 and 4).

The resistors for the voltage dividers were manufactured by the Shallcross Manufacturing Co. Each divider consisted of twenty-five one megohm two watt resistors and a 750 ohm tap resistor. The resistors were of 1% accuracy and 0.01% stability.

One of these one megohm resistors was chosen as a standard and the ratio of each of the fifty resistors in the divider to the standard was measured with a simple circuit containing a Leeds and

*Cf. Accompanying Technical Report.

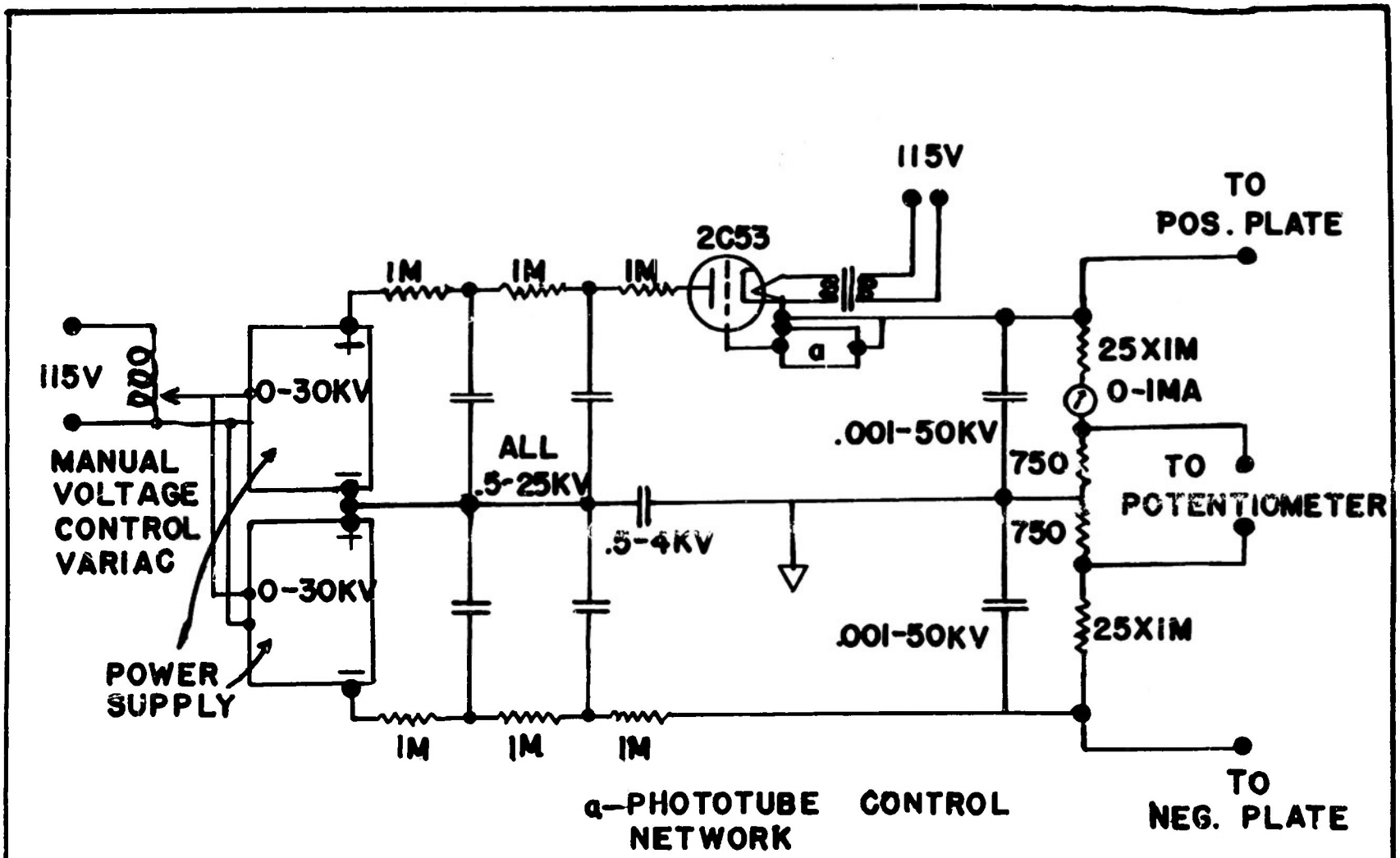

VOLTAGE SUPPLY FOR ANALYZER PLATES

FIGURE 3

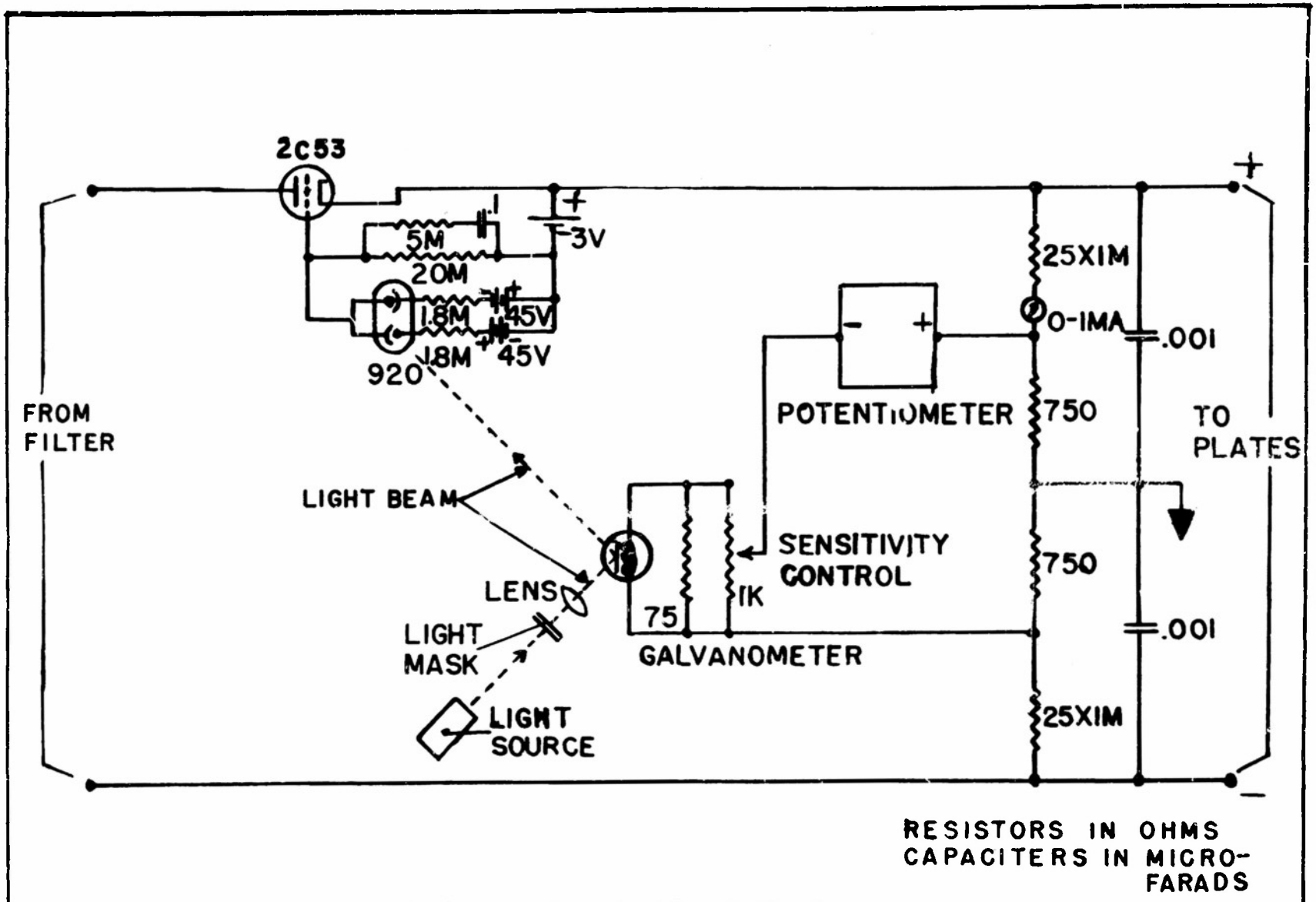

VOLTAGE MEASURING AND STABILIZING CIRCUITS

FIGURE 4

Northrup type K potentiometer and a Vibrating Reed Electrometer as a null detector. The sum of the ratio of the fifty resistors to the standard was found to be: 49.9548 ± 0.01%. The two 750 ohm tap resistors were connected in series and their ratio to the standard one megohm was measured. This was done in two steps through two precision resistors (10K and 100K) in order to keep the resistance ratios to a maximum of ten. From these ratios the ratio of the fifty one megohm resistors (called R_{50M}) to the two 750 ohm tap resistors (called R_{1500}) is

$$\frac{R_{50\ M}}{R_{1500}} = 3.3280 \times 10^4 \pm 0.02\% \tag{5}$$

The voltage between the analyzer plates was therefore

$$V = V_{pot} \times \frac{R_{50\ M}}{R_{1500}} \tag{6}$$

Strictly, one should have found the ratio $\frac{R_{50\ M} + R_{1500}}{R_{1500}}$. However, the addition of 1500 ohms to 50 megohms would have increased the 50 megohms by 0.003%.

The resistor temperature coefficient was 0.002% per degree C. A test voltage of 1000 volts applied to one of the 1 M resistors produced a temperature change of 20°C, or an increase of resistance of 0.04%. Since 700 volts was the largest voltage drop per resistor needed during the photodisintegration experiments, the maximum error in the voltage divider ratio due to resistor temperature coefficient was approximately 0.02%. This error would result if the tap resistance did not change value due to heating, and in the more likely event of increase of tap resistance during operation, the above error would be reduced.

The voltage divider resistors were mounted in groups of three between corona-free shields supported by 1" Lucite insulating columns. Each stack assembly was inclosed in a 7" diameter Lucite cylinder 24" high, similar to the method of Henkel and Petree[10]. The whole assembly was sealed after a dessicant had been placed inside, so that changes in humidity would not affect the resistance values. A blower circulated air inside the stacks.

The potentiometer used to measure the voltage across the tap resistors was a Rubicon Portable Precision Potentiometer. The limit of error of the potentiometer was the voltage corresponding to one slide wire division plus 0.05% of the voltage reading of the dial switch. The potentiometer was checked against a Bureau of Standards checked standard cell of e.m.f. 1.01918 volts. The potentiometer measured this as 1.01895 volts, a difference of 0.02%. However, an accuracy of $\pm$ 0.05% was assumed for the potentiometer.

The final formulas for the voltage between the analyzer plates is given by

$$V = (V_{pot} \pm 0.05\%)(3.3280 \times 10^{4} \pm 0.02\%)$$

$$V = (3.3280 \times 10^{4})\ V_{pot} \pm 0.054\% \qquad (7)$$

The voltage supply for the analyzer plates was composed of two 0-30 kv power supplies, additional filters, the previously-described resistor voltage dividers, and a stabilizing network. The circuit diagram is shown in Figure 3. The power supplies were manufactured by Condenser Products Company and were rated at 1 ma output current. Their filtering was insufficient for the present experiment, the percentage of 120 cycle ripple being about 5%. Two sections of R-C filtering placed at the output of each power supply resulted in a theoretical attenuation of ripple by a factor of 10^{5}.

In series with the output of the positive supply was a series regulator tube, followed by the positive voltage divider to ground and from ground the negative voltage divider to the negative voltage supply. Across the two 750 ohm tap resistors was connected the Rubicon potentiometer in series with a Leeds and Northrup type HS galvanometer. (Sensitivity - 0.5 $\frac{\mu ar}{mm}$; Period - 1.4 sec.)

The galvanometer was used in a feedback loop to stabilize the voltage between the analyzer plates. Light from a lamp was reflected from the galvanometer mirror and focussed on the cathodes of the twin phototube, type 920, in the grid circuit of the series regulator tube. A mask was placed in the light beam so that a shadow was cast on half of one phototube cathode and another shadow cast on the opposite half of the other cathode. With no current flowing in the galvanometer the illuminated areas of the two cathodes were equal, and hence no current flowed in the external load resistor. Current flow through the galvanometer resulted in a movement of the shadow pattern, causing more illumination on one cathode than on the other and therefore causing a voltage drop across the load resistor. This voltage drop changed the grid bias of the regulator tube and hence changed the voltage across the dividers in a degenerative sense. The gain of the feedback loop depended on three factors: the length of the light path, the intensity of illumination, and the sensitivity of the galvanometer. The first factor was fixed at a value of approximately three feet. The intensity of illumination was conveniently adjusted by means of a Variac in the voltage source for the lamp. The galvanometer sensitivity was controlled by a resistor potentiometer connected as an Ayrton shunt.

An anti-hunt circuit was incorporated in the grid circuit of the regulator tube. Without some such circuit the transient response of the system was oscillatory for high gain, whereas if the gain was reduced to reduce the tendency for oscillation, then the stabilizing effect of the system was reduced. The constants were chosen experimentally for optimum response.

The stabilization of the analyzer voltage effected by this feedback system and by deriving the input A.C. power from a Sorensen Regulator was such that, with no beam through the analyzer, the voltage varied less than 3 volts out of 30,000 volts, a factor of 0.01%. During operation, small breakdowns would cause the voltage to jump at times, but the average stabilization was of the order of 0.02 or 0.03%.

The power supply and resistor dividers were mounted in the bottom of a carriage which supported the surface plate. Electrical connection from the supply to the analyzer plates was through bakelite bushings inserted through holes in the surface plate.

III MAGNETIC FIELD

Although the instrument was designed as an electrostatic analyzer, in any precision experiment of this type the effect of magnetic fields must be considered. The component of this field directed from one plate to the other (called radial component) produced beam deflection perpendicular to the plane of the analyzer. Deflection in this direction would not affect the accuracy of the experiment, but would tend to throw the beam out of the analyzer. On the other hand, the component of magnetic field perpendicular to the plane of the analyzer (called vertical component) would

produce deflections in the plane of the analyzer, i.e., in the same plane as deflections due to the electric field. Hence the vertical component either had to be known accurately so that its deflecting effect could be added to the electric field deflection; or it had to be reduced to such a value that it contributed negligible deflection. The latter method was attempted.

After machining, the analyzer plates exhibited a high degree of magnetism non-uniformly distributed. In the first demagnetization attempts, the plates were wound with many turns of wire, and 60 cycle current passed through. The current magnitude was slowly decreased by means of a Variac from several amperes to zero. This degaussing process resulted in a decrease of magnetic field at the worst point between the plates to about 7 gauss.

Ellithorn and Angelakos[11] have shown that the demagnetization of ferromagnetic materials of large cross-sectional area was best accomplished by the use of alternating current of low frequency, of the order of two cycles per second. The final degaussing method used this principle. Two horseshoe electromagnets were placed across the ends of the analyzer plates, spanning the analyzer gap, so that the two plates completed a series magnetic circuit. Square waves of current were passed through the two electromagnet coils in series. One end of the coils was returned to the center tap of a battery, while the other end was switched from one end of the battery to the other. Switching was accomplished by a cam and switch driven by a low speed motor. The switching rate was approximately once per second. Degaussing current was very slowly decreased from several milliamperes to zero by means of a rheostat

in series with the coils. After several repetitions of this procedure the average value of the vertical component of magnetic field in the gap was reduced to an acceptably small figure.

The magnetic field was measured by two methods, one used before the threshold determinations, the other used afterward. In the first method, the measurement of the magnetic field in the gap was made with a flip coil and ballistic galvanometer.

In the second method the magnetic field was measured by the peaking strip method and has been described by Bhattacherjee, Waldman and Miller[9]. The results of the two methods are in good agreement even though the measurements were spaced many months apart. Presumably the magnetic field is stable.

A plot of the vertical component of the magnetic field is shown in Figure 5. The analysis of Honnold and Miller[7] shows that the effect of the magnetic field is to deflect the beam passing through the analyzer toward larger radius of curvature. Thus the value of the kinetic energy computed by use of Eq. 2 must be reduced. The corrections are 3.5 kev for the deuterium threshold and 3.4 kev for the beryllium threshold.

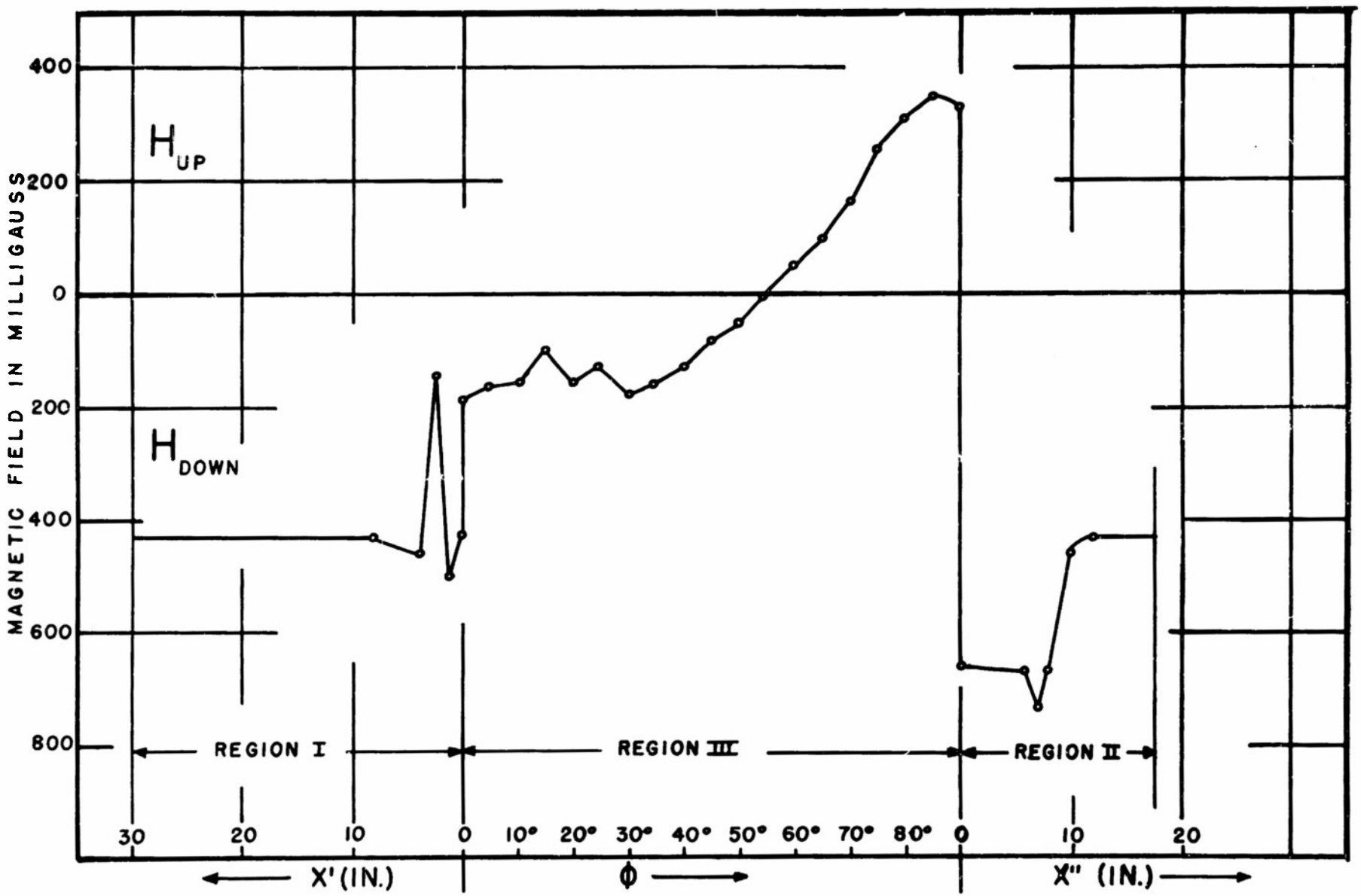

FIG. 5 MAGNETIC FIELD DISTRIBUTION

SUMMARY OF ERRORS

Ratio of separation of plates to mean radius (d/a)		
Inner radius (r_1)		0.005%
Outer radius (r_2)		0.005%
Mean radius (a)		0.01 %
Separation of plates (d)		0.05 %
	Total	0.05 %
Voltage Measurement		
Voltage divider ratio		0.02 %
Potentiometer		0.05 %
Voltage Stabilization		0.03 %
	Total	0.06 %
Magnetic field correction		
Correction of 3.5 kev $\pm$ 10%		0.02 %
	Grand Total	0.08 %
Energy resolution due to slit widths	(at 2.23 Mev)	0.13 %
	(at 1.66 Mev)	0.12 %

IV EXPERIMENTAL PROCEDURE

The general plan of the electrostatic generator, analyzer, and counters is shown in Figure 6. The target was a 1/16" gold disk, a "thick" target for the energies under consideration. The material to be disintegrated, beryllium or deuterium oxide, was placed in a cavity in a cylindrical lead shield, of 6" outer diameter and 8½" length. The cavity containing the sample was 3¼" in diameter and 7" long, concentric with the cylinder. A 3/4" hole was drilled along the cylinder axis, from the base to the cavity.

The lead shield, containing the sample, was oriented with its axis horizontal, and pushed up to the gold target so that the target projected approximately 3/8" inside the cavity. By shielding in this manner, only x-rays from the direction of the target could disintegrate the sample.

The lead shield was encased in a block of paraffin 10" x 11" x 15". The BF_3 (enriched boron 10) neutron counter was inserted in a hole in the paraffin directly above the target and sample, with its axis horizontal and perpendicular to the direction of the beam. By placing the counter above the target, the highly forward-directional x-rays from the target caused little background in the counter.

A Geiger counter was located directly behind the 3/4" hole in the lead shield. It was well shielded by lead from all directions except on the line to the target. The Geiger counter was used to monitor the x-rays from the target.

For the beryllium disintegration experiment, a cylinder of

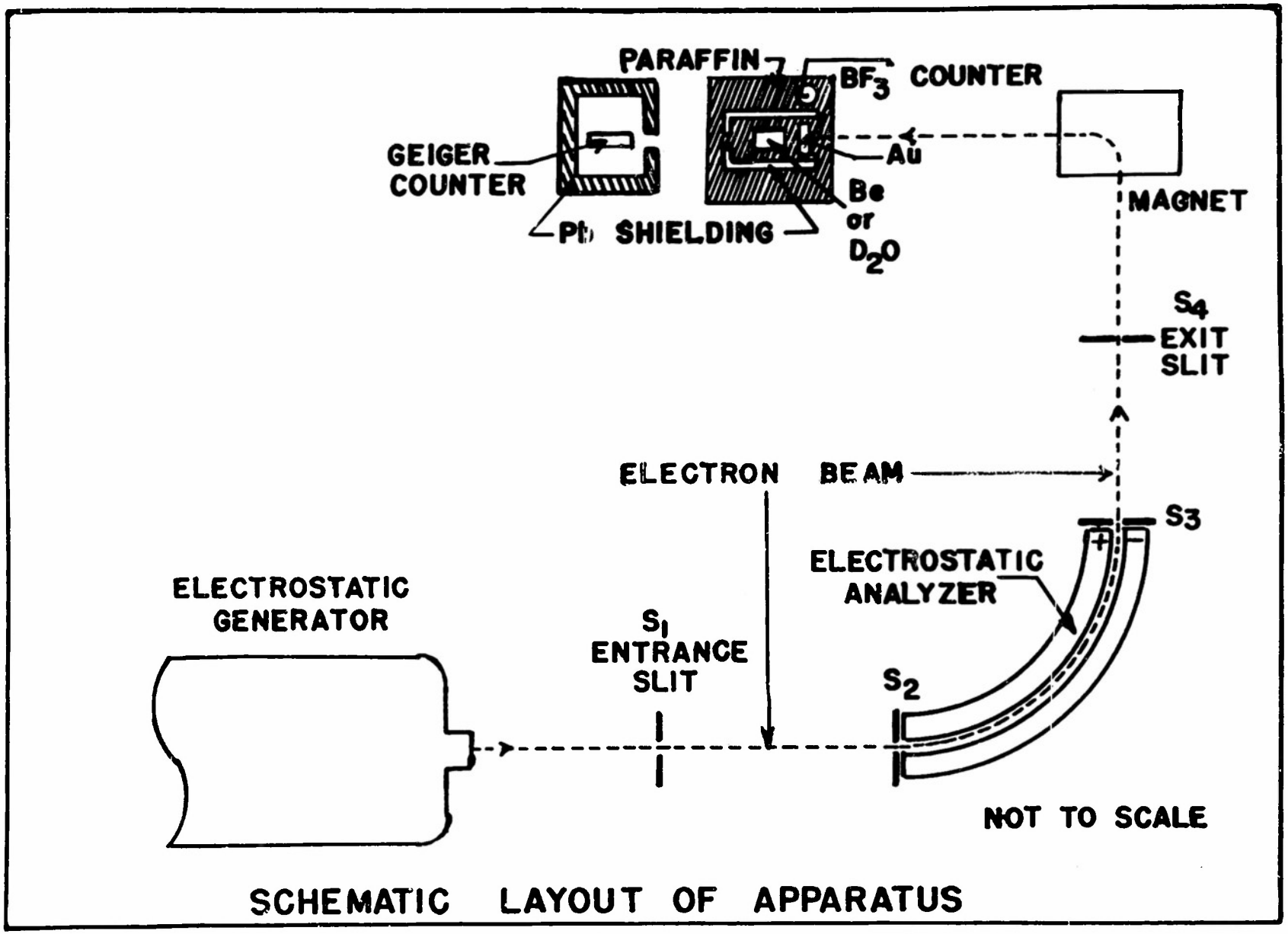
PARAFFIN
BF_3 COUNTER
GEIGER COUNTER
Au
Be or D_2O
Pb SHIELDING
MAGNET
S_4 EXIT SLIT
ELECTRON BEAM
S_3
ELECTROSTATIC ANALYZER
ELECTROSTATIC GENERATOR
S_1 ENTRANCE SLIT
S_2
NOT TO SCALE
SCHEMATIC LAYOUT OF APPARATUS

FIGURE 6

Be 2" in diameter and 2" long, weighing 192 grams, was placed in the shield next to the target. The potentiometer was set for a voltage corresponding to an electron beam energy approximately 30 kev above threshold, and, with the feedback galvanometer completely shunted, the analyzer voltage was brought up by means of a Variac in the primary of the power supplies until the potentiometer was balanced. The sensitivity of the galvanometer was then increased to an optimum value. The beam from the electrostatic generator was then directed into the analyzer, the current distribution on slits S_1 and S_2 helping to determine when the beam was going in straight. The sphere voltage was adjusted until current passed through the analyzer, as evidenced by current on S_3 and S_4. At this point the energy of the electron beam was known to within the resolution of the analyzer, as determined by the widths of slits S_1 and S_4. For the beryllium experiment a resolution of 2 kev was used, which (M = -0.755 at 1.67 Mev) required slit widths of 0.041" and 0.031" for S_1 and S_4 respectively.

The beam impinging on the gold target produced bremsstrahlung. A sufficient number of monitoring x-ray counts was taken to insure good statistical accuracy. The number of neutron counts in the time required to accumulate a standard number of x-ray counts was then recorded. This number of neutron counts, less background, furnished one point on the yield curve.

To get the next point, the voltage on the analyzer was reduced by the equivalent of 3 kev and the generator potential decreased until current again was passed by the analyzer. To change the analyzer voltage it was sufficient merely to change the potentiometer

to the new setting, the high gain of the stabilizer causing the analyzer voltage to follow. At this new voltage the neutron counts for the standard number of x-ray counts were again recorded. This process or run was continued to below threshold, where only background neutrons were recorded. (Background ca 20 counts/1000 sec.)

The target assembly was originally installed just beyond the image slit S_4. It was found that when the sphere voltage was slightly high, so that the beam entered the analyzer but struck the outer half of slit S_3, a greater number of neutron counts was recorded than when the beam was directed down the middle. This was caused by x-rays from slit S_3 disintegrating the sample. To eliminate this the target was moved to the position shown in Figure 6, adequate shielding being interposed between slits S_3 and S_4 and the sample. The necessary change in direction of the beam was effected by the indicated electromagnet. This magnet served merely to change the beam direction by 90°, and was not used in energy determination. It was located 49" from S_4, a distance great enough so that its small stray field would have no effect on the beam in the analyzer. The target was 14" from the exit edge of the magnet.

The disintegration of deuterium was carried out in the same manner as for the beryllium. The sample was 130 grams of heavy water, D_2O, 99.9% pure, sealed in a brass container. A resolution of 3 kev at 2.2 Mev was obtained by opening slits S_1 and S_4 to 0.063" and 0.048" respectively (M = -0.770 at 2.22 Mev).

A greater slit opening was found necessary at the higher energy because of the poorer stability of the voltage of the

electrostatic generator. The generator potential was stabilized by both a capacitive stabilizer[12] and a slow-acting spray voltage regulator[13], which together maintained an average longtime generator stability of about $\pm 0.4\%$. A poor stability required a longer period of time to obtain a given normalizing x-ray count, and hence meant a larger background count in the Geiger counter, with greater attendant errors.

V THEORY

The deuteron problem is well known and has been solved exactly as far as the limits of error in this experiment are concerned. Bethe[14] in a summary of the work done on the problem shows that the deuteron near threshold is photo-magnetically disintegrated. He gives the following expression as the photo-magnetic disintegration cross section:

$$\sigma_m = \frac{2\pi}{3} \frac{e^2}{\hbar c} \frac{\hbar^2}{M} \frac{\sqrt{W_1}\sqrt{E}\left(\sqrt{W_1}+\sqrt{W_0}\right)^2}{(E+W_1)(E+W_0)Mc^2}\left(\mu_p-\mu_N\right)^2 \qquad (12)$$

where $E = h\nu - W_1$, W_1 is the deuteron binding energy, W_0 is the fictitious binding energy for the singlet state, and μ_N and μ_p are the nuclear magnetic moments of the neutron and proton respectively. This expression involves E which has a definite value for a given incident x-ray energy. We are concerned with all x-ray energies in the energy interval between threshold and the energy of the electrons. We call this interval "y" and integrate this cross section over "y".

$$\sigma_x = \frac{2\pi}{3} \frac{e^2}{\hbar c} \frac{\hbar^2}{M} \int_0^y \frac{\sqrt{W_1}\sqrt{E}\left(\sqrt{W_1}+\sqrt{W_0}\right)^2}{(E+W_1)(E+W_0)Mc^2}\left(\mu_p-\mu_N\right)^2 dE \qquad (13)$$

The result is:

$$\sigma_\chi = k' \left[4638.22\, y^{\frac{1}{2}} + (3297.78\, y - 6500.5023) \tan^{-1} 0.671156\, y^{\frac{1}{2}} - (1088.485\, y + 69.66304) \tan^{-1} 3.9528050\, y^{\frac{1}{2}} \right] \qquad (14)$$

where σ_χ is a measure of the total probability of a disintegration taking place and k' is a slowly varying function of the incident x-ray energy and is a constant over the range of energies under consideration. It should be noted that this expression is dependent only on "y". A plot of σ_χ / k' against "y" on log-log paper results in a straight line with a slope of 2.365.

Since sigma is a measure of the total probability of a disintegration taking place, it is also directly proportional to the neutron yield in the experiment. A linear plot of the 2.365th root of the neutron yield against the electron beam energy should result in a straight line. The extrapolation of this line to zero neutron yield determines the threshold energy.

In applying the above theoretical relations the energy must be referred to the center of mass system. In the case of deuterium 1.3 kev must be subtracted from the electron energy (for the 30 kev interval).

The binding energy of deuterium can be used along with mass spectroscopic data to determine the mass of the neutron. Using the HH-D mass difference from spectroscopic data in conjunction with the n + H - D mass difference (deuteron binding energy) as determined by this experiment, a figure for the n-H mass difference is obtained.

Since the mass of the hydrogen nucleus is well known, the mass of the neutron can be determined.

Because of the complexity of the beryllium nucleus, the situation viewed from the theoretical standpoint is not nearly so clear-cut as in the case of deuterium. Guth and Mullin[15] developed the photodisintegration cross section for Be^9. Making the proper approximations due to near-threshold energies in their expression and integrating over "y" gives:

$$\sigma_n = A f(E_i) \int_{E_o}^{E_i} (E - E_o)^{1/2} (E_i - E)\, dE$$
$$= B (E_i - E_o)^{5/2} = B\, y^{5/2} \qquad (15)$$

where E_i is the energy of the incident electron beam, E is the x-ray energy, E_o is the threshold energy, $f(E_i)$ is a slowly varying function of energy and is constant over y, and A and B are constants. σ_n is a measure of the total probability of a disintegration taking place and is therefore directly proportional to the neutron yield in a disintegration experiment. Thus theory predicts that the neutron yield should vary directly as the 5/2 power of "y".

As mentioned above it is necessary to subtract a center of mass correction of 0.2 kev.

VI EVALUATION OF DATA

Using the procedure described in the experimental section six runs were made to determine the binding energy of beryllium. Slit widths corresponding to 2 kev resolution of the beam energy were used. Because of this, 2 kev steps in beam energy from 20 kev above threshold down to threshold were used.

Each run was plotted individually on a log-log plot and the best straight line for the 20 kev beam variation was chosen. The average slope of these straight lines was close to 2 instead of the theoretical value of 2.5. Because of this the square root of the neutron yield was plotted against beam energy on a linear plot and these straight lines extrapolated to zero neutron yield to determine the threshold.

Fig.7 is a plot of neutron yield vs. corrected electron energy* The correction consisted of -3.4 kev for the magnetic field effect and -0.2 kev for the motion of the center of mass. Fig. 8 is a plot of the square root of the neutron yield vs. corrected electron energy. Table 6 summarizes the determination of the binding energy from the data.

Table 6

Run Number	1	2	3	4	5	6
Binding Energy	1.6640	1.6624	1.6617	1.6606	1.6606	1.6598

Average 1.662 $\pm$ .003 Mev

The internal consistency of these data is not as good as that for the deuterium determination nor does the yield follow the theoretical 2.5 power. In virtue of this we do not feel justified in attaching an error of less than 3 kev to the binding energy.

Four runs were made to determine the binding energy of deuterium. A run consisted of measuring the neutron yield at various beam energies from 35 kev above threshold down to threshold. Five kev steps in beam energy in the upper energy region and three kev steps

*Size of circles is greater than standard deviation of counting statistics.

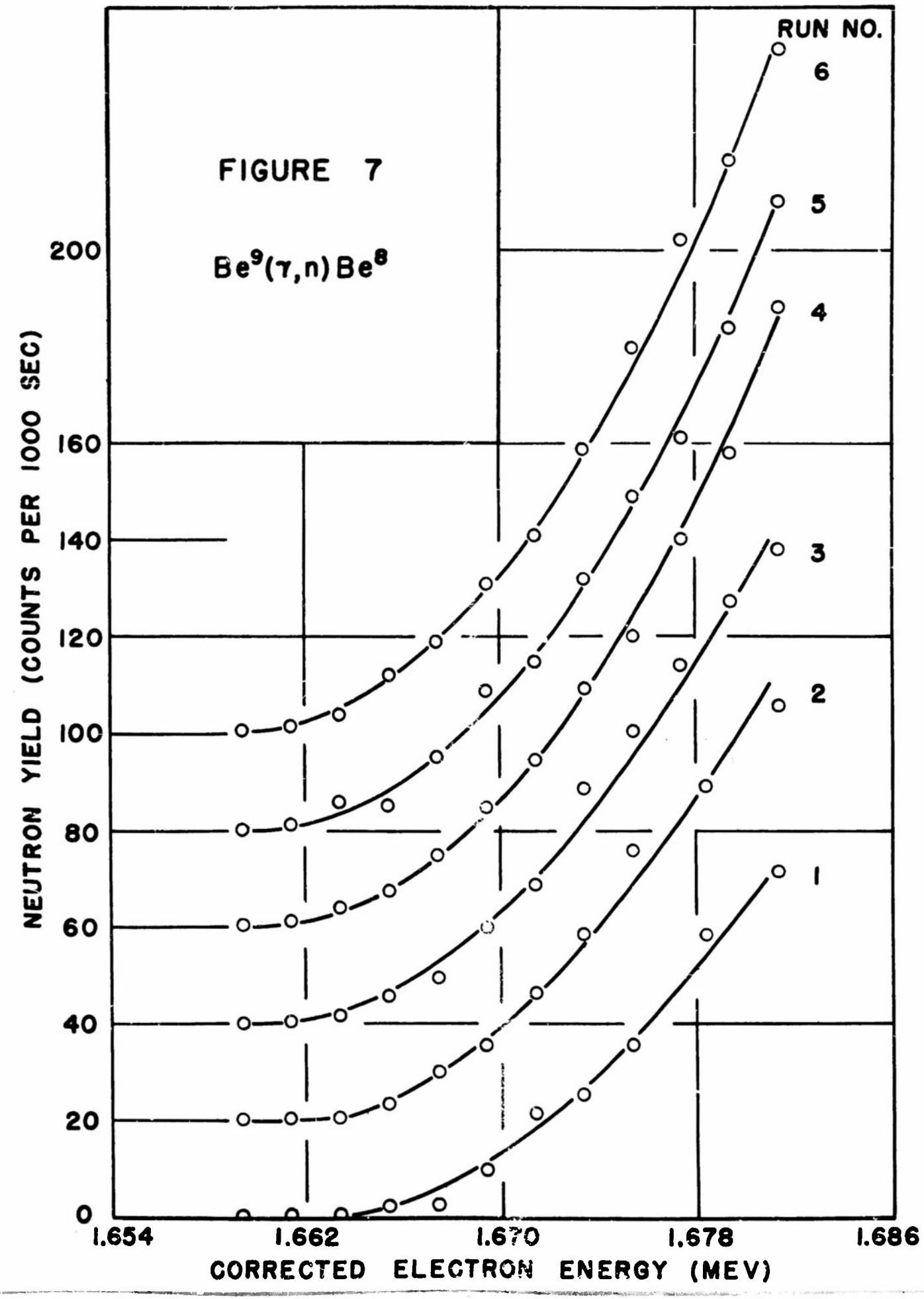
FIGURE 7
$Be^9(\gamma,n)Be^8$
RUN NO.
6
5
4
3
2
1
NEUTRON YIELD (COUNTS PER 1000 SEC)
0
20
40
60
80
100
120
140
160
200
1.654
1.662
1.670
1.678
1.686
CORRECTED ELECTRON ENERGY (MEV)

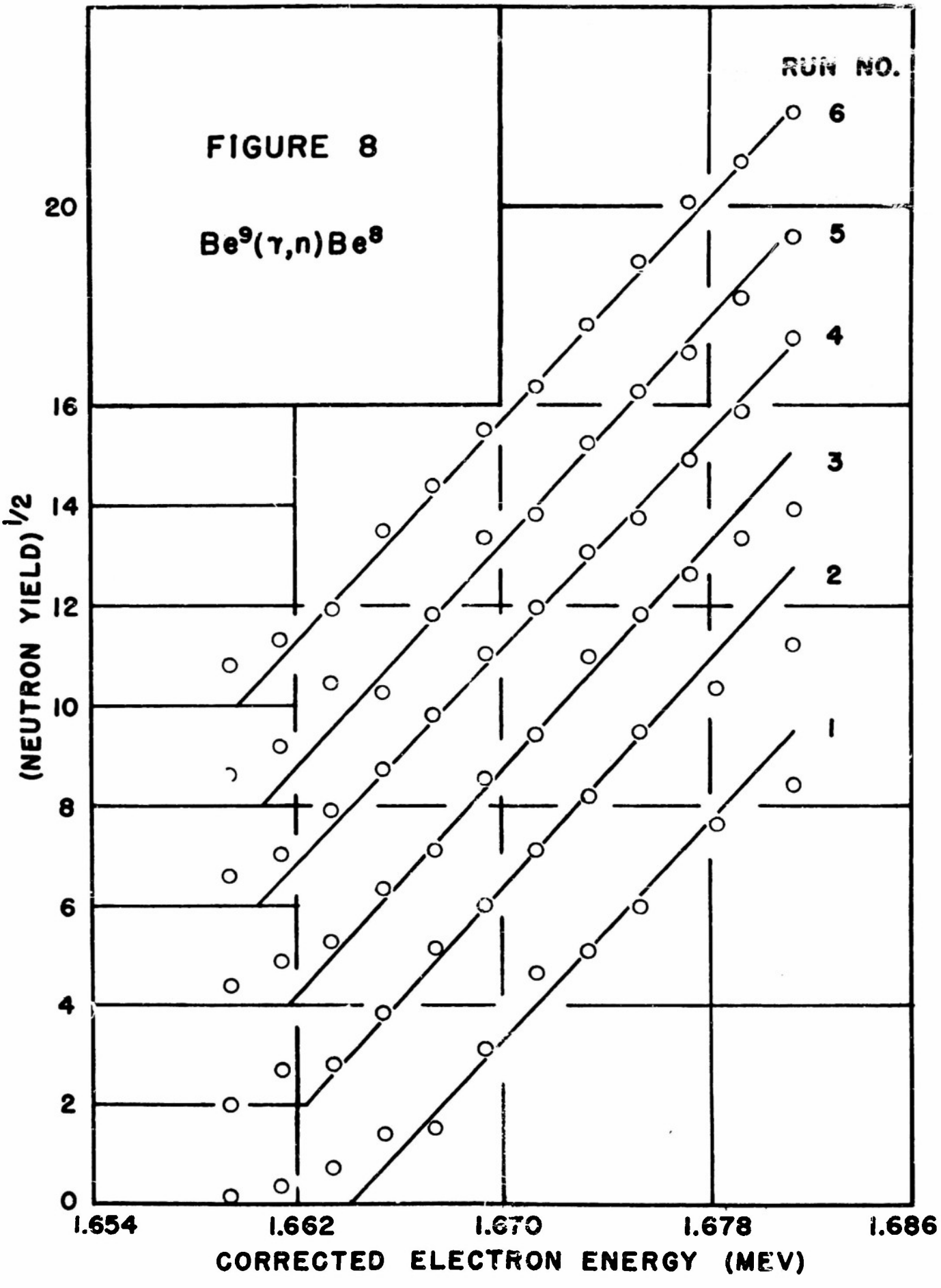
FIGURE 8
$Be^9(\gamma,n)Be^8$
RUN NO.
6
5
4
3
2
1
(NEUTRON YIELD)$^{1/2}$
0
2
4
6
8
10
12
14
16
20
1.654
1.662
1.670
1.678
1.686
CORRECTED ELECTRON ENERGY (MEV)

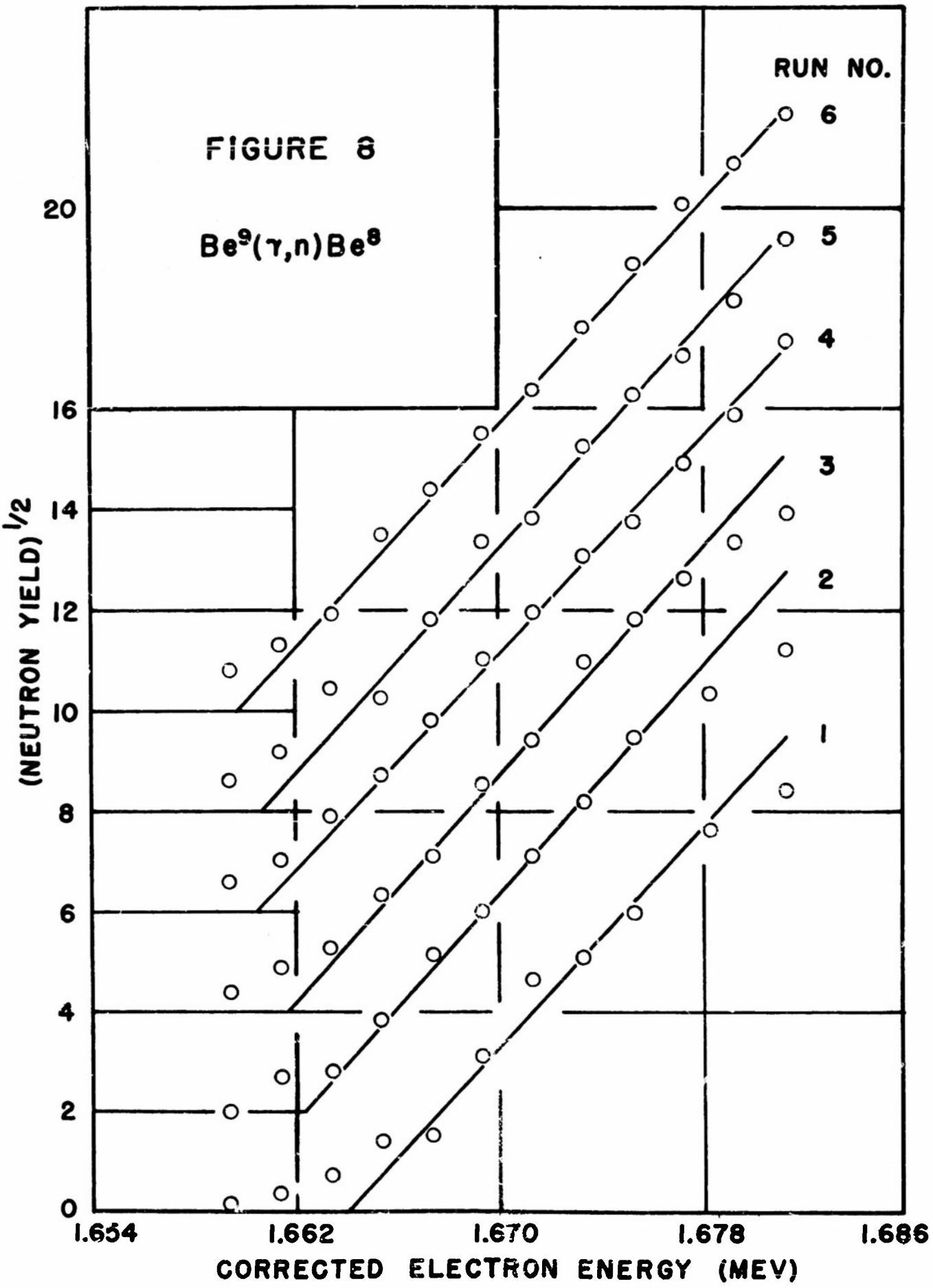
FIGURE 8
$Be^9(\gamma,n)Be^8$
RUN NO.
6
5
4
3
2
1
20
16
14
12
10
8
6
4
2
0
(NEUTRON YIELD)$^{1/2}$
1.654
1.662
1.670
1.678
1.686
CORRECTED ELECTRON ENERGY (MEV)

in the lower energy region were used. Each run was analyzed individually using the methods outlined in the theoretical section.

Fig. 9 is a plot of neutron yield vs corrected electron energy. The correction consisted of -3.5 kev for the magnetic field effect and -1.3 kev for the motion of the center of mass. Fig. 10 is a plot of the 2.365th root of the neutron yield vs. corrected electron energy. In an attempt to use another method for the location of the threshold a log-log plot of neutron yield vs. excess electron energy was made[4]. In the region of the log-log plot which distinguished between possible thresholds, the errors associated with each point were so large on the log scales as to obliterate the distinction.

Table 7 summarizes the determination of the binding energy from these figures.

Table 7

Run Number	1	2	3	4
Binding Energy	2.2270	2.2272	2.2271	2.2270

Average 2.227 ± .003 Mev

The results of the four runs show a much better internal consistency than that indicated by the stated error of 3 kev. As shown in the experimental section the limiting error in this experiment was the energy resolution of the analyzer. This energy resolution was determined by the slit openings used, and was ± 3 kev in this case.

In August of 1951, Li et al[16] published a compilation of the work done up to that time in measuring nuclear disintegration

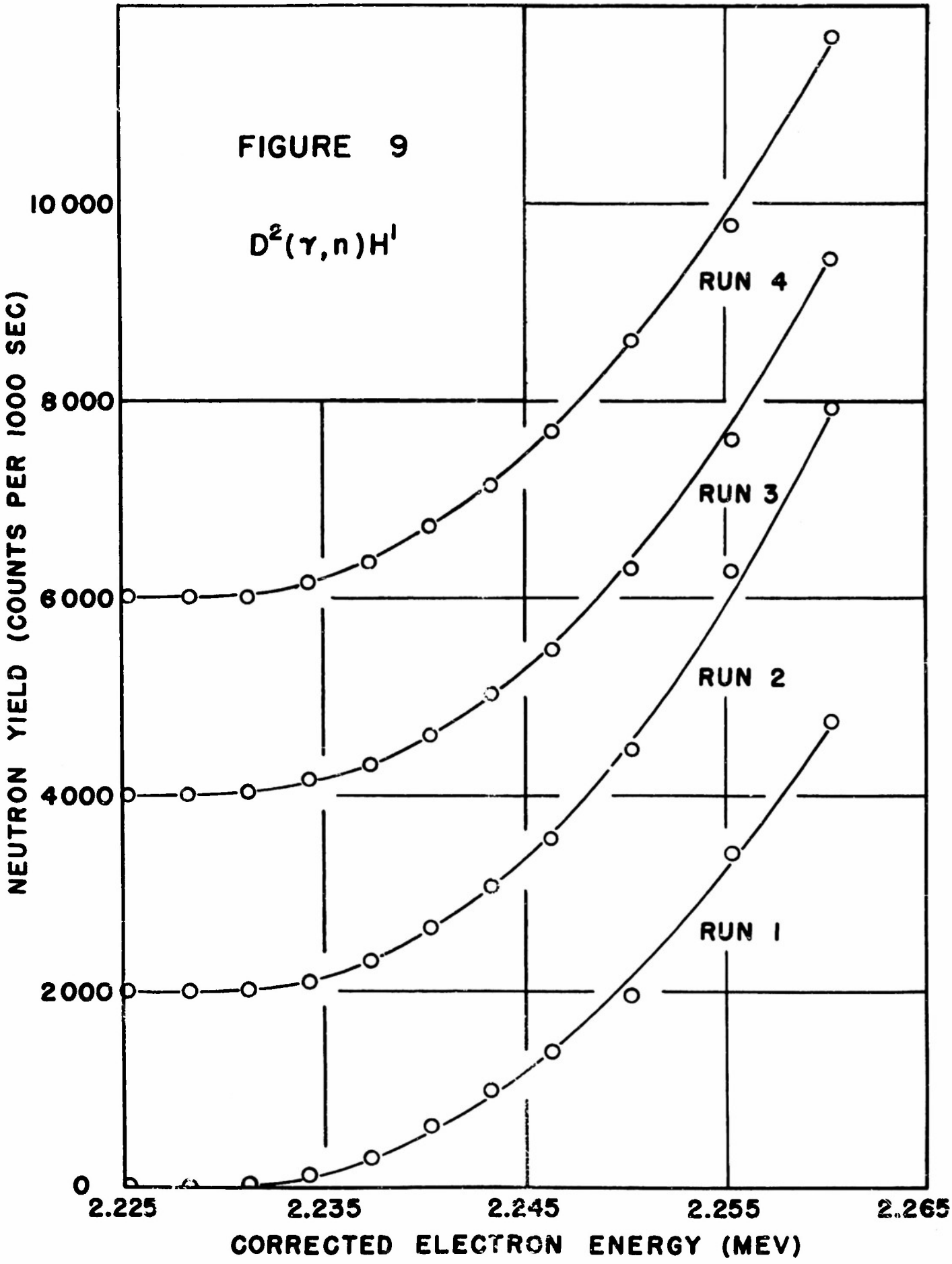
FIGURE 9
$D^2(\gamma,n)H^1$
NEUTRON YIELD (COUNTS PER 1000 SEC)
10 000
8000
6000
4000
2000
0
RUN 4
RUN 3
RUN 2
RUN 1
2.225
2.235
2.245
2.255
2.265
CORRECTED ELECTRON ENERGY (MEV)

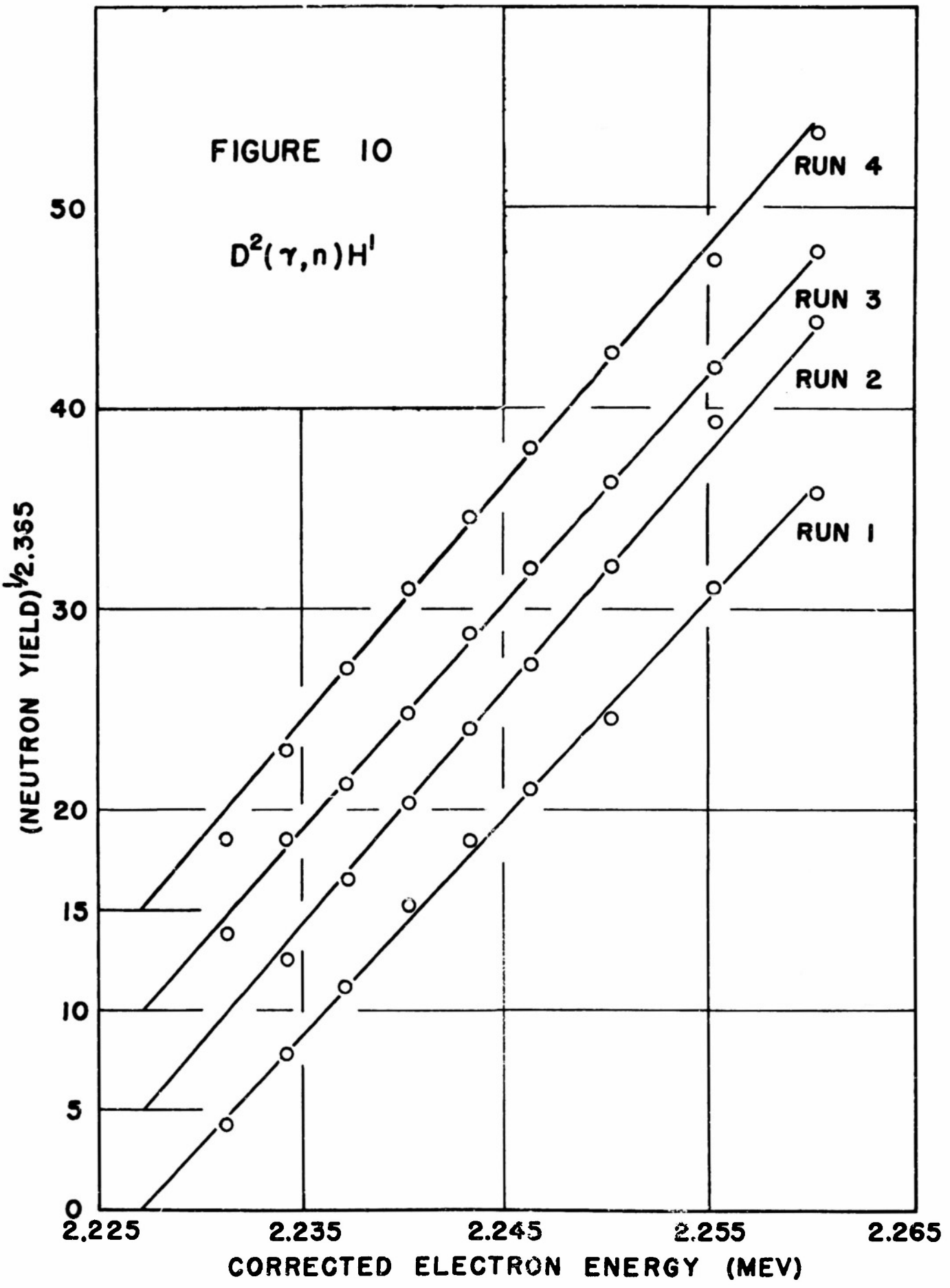
FIGURE 10
$D^2(\gamma,n)H^1$
RUN 4
RUN 3
RUN 2
RUN 1
(NEUTRON YIELD)$^{1/2}$.355
0
5
10
15
20
30
40
50
2.225
2.235
2.245
2.255
2.265
CORRECTED ELECTRON ENERGY (MEV)

energies of light nuclei. They considered only recent experiments and their value for the binding energy of deuterium is a weighted mean of all the nuclear experiments measuring that binding energy directly. Van Patter[17] in January of 1952, extended the work of Li. He published a weighted mean for the direct experimental determinations of binding energy that included a preliminary Notre Dame figure which neglected the magnetic field corrections[18]. Both Li and Van Patter published a binding energy figure determined as an internally consistent weighted mean of all the nuclear cycles involving light nuclei that could be combined to give n + H - D. Their figures, along with those of Bell and Elliott, and Mobley and Laubenstein, are presented in Table 8.

Table 8

	B.E. of Deuterium	B.E. of Beryllium
Notre Dame	2.227 ± 0.003 Mev	1.662 ± 0.003 Mev
Bell & Elliott	2.230 ± 0.007	
Mobley & Laubenstein	2.226 ± 0.003	1.666 ± 0.002
Li et al (weighted exp. mean)	2.227 ± 0.002	1.666 ± 0.002
Van Patter (weighted exp. mean)*	2.228 ± 0.002	1.665 ± 0.002
Li et al (internally consistent mean)	2.226 ± 0.002	1.666 ± 0.002
Van Patter (internally consistent mean)	2.226 ± 0.002	1.666 ± 0.002

*Includes preliminary Notre Dame values of 2.231 and 1.664 Mev.

Using the HH - D mass difference of 1.445 ± 0.002 Mev from mass spectroscopic data[19], and our binding energy of deuterium, n - H difference is 782 ± 4 kev. This, together with the atomic mass of hydrogen[16], leads to a value of 1.008982 for the mass of the neutron.

In order to check the accuracy of our electrostatic analyzer, Bhattacherjee, Waldman and Miller[9] measured the conversion electron energy accompanying the disintegration of Ba^{137}. Their value for the transition energy of 662.6 ± 0.9 kev is in good agreement with the 661.60 ± 0.14 kev value of Muller, Hoyt, Klein and Dullond[20], and the 661.65 ± 0.15 kev value of Lindstrom, Siegbahn and Wapstra[21].

1. W. E. Stephens, Rev. Mod. Phys., 19, 19 (1947)

2. R. E. Bell and L. G. Elliott, Phys. Rev., 79, 282 (1950)

3. J. L. Wolfson, Phys. Rev. 78, 176 (1950)
W. L. Brown, Phys. Rev. 85, 271 (1951)
G. Lindstrom, Phys. Rev. 87, 678 (1952)

4. R. C. Mobley and R. A. Laubenstein, Phys. Rev., 80, 309 (1950)

5. Herb, Snowden, and Sala, Phys. Rev., 75, 246 (1949)

6. K. T. Bainbridge, Experimental Nuclear Physics, Vol. I.
E. Segre, Editor (John Wiley and Sons, Inc. New York, 1953)

7. V. R. Honnold and W. C. Miller, Nuclear Physics Technical Report No. 2, University of Notre Dame (1953)

8. R. Herzog, Zeit f. Physik, 89, 447 (1934)
Zeit. f. Physik, 97, 596 (1935)
Phys. Zeit., 41, 18 (1940)

9. Bhattacherjee, Waldman and Miller, Nuclear Physics Technical Report No. 4, University of Notre Dame (1953)

10. R. L. Henkel and B. Petree, Rev. Sci. Inst., 20, 720 (1949)

11. H. E. Ellithorn and D. J. Angelakos, Am. Jour. Phys., 13, 390 (1945)

12. Miller, Waldman, Noyes and Van Hoomissen, Phys. Rev., 77, 758 (1949)

13. A. O. Hanson, Rev. Sci. Inst., 15, 57 (1944).

14. H. A. Bethe, Elementary Nuclear Theory (John Wiley and Sons, Inc., New York, 1947)

15. E. Guth and C. J. Mullin, Phys. Rev., 76, 234 (1949)

16. Li, Whaling, Fowler, and Lauritsen, Phys. Rev., 83, 516 (1951)

17. D. M. Van Patter, MIT Technical Report #57 (1952)

18. Noyes, Van Hoomissen, Miller and Waldman, Phys. Rev. 85, 727 (1952)

19. T. R. Roberts, Phys. Rev. 81, 624 (1951)

20. Muller, Hoyt, Klein and DuMond, Phys. Rev. 88, 775 (1952)

21. Lindstrom, Siegbahn and Wapstra, Proc. Phys. Soc. B, 66, 54 (1953).